A Low-Cost, High-Speed, High-Resolution, Adaptively Tunable Microwave Network for an SDR UHF RFID Reader Reflected Power Canceller

Edward A. Keehr
Superlative Semiconductor LLC, Carlsbad, CA, United States of America
Email: keehr@super-semi.com

***Abstract*—A key problem with custom built and software-defined RFID reader architectures is that the large continuous-wave (CW) signal that must be transmitted during RFID tag reading must be concurrently processed by the RFID receive (RX) chain. Methods for handling this signal that are easily implemented in custom RFID reader ASICs are not typically inherently available in low-cost commercial off the shelf components. In this paper, a subranging digitally-tunable capacitor approach to reflected power cancellation in a low-cost software-defined RFID reader to address this issue is described. The key components of the proposed architecture cost under $4 in bulk and together consume less than 1mA quiescent current. The subranging aspect of the tunable microwave network providing the variable reflection coefficient reduces the residual cancellation error of the network by 30dB over the non-subranging case. The resulting network improves the TX leakage signal at the SDR ASIC RX input by 50dB over the uncancelled case and can be driven by an adaptive cancellation algorithm that converges in a median time of less than 10ms.**

I. Introduction

A. Background

The requirement to remove transmit leakage at the RFID reader receiver (RX) stems from the need to have the RFID reader power the passive tag with a large transmit (TX) signal while the tag is communicating back to the reader. In general radio systems, the problem of handling concurrent large TX and small RX power is traditionally solved through the use of a duplexer at the antenna to provide isolation between the two channels in the radio. However, this technique requires significant frequency separation between TX and RX frequencies. In order for the tag to draw a minimal amount of power while maximizing its backscatter signal energy, significant frequency translation of the tag response from the transmitted carrier is challenging and for the purposes of the UHF RFID EPC Gen 2 specifications is not done at all [1].

Simply filtering out the TX leakage at RX baseband with a DC notch or HPF is likewise an insufficient strategy. First, such a facility may not even be available prior to the ADC in the chosen RFID reader components. Second, unless the RX downconversion mixer is driven by the TX local oscillator or the TX output signal itself [2], the in-band phase noise generated by mixing the large TX signal with the RX LO can easily overwhelm the desired tag backscatter signal intended for reception. In many cases, the TX interference problem is partially solved by separating the transmit and receive antennas of the RFID reader in what is termed a bistatic configuration. However, a monostatic reader, in other words a reader with a shared antenna between TX and RX, is often preferred to reduce the cost and size of the reader. For all of these reasons, explicit cancellation of the TX leakage within the reader receiver at RF is highly desirable.

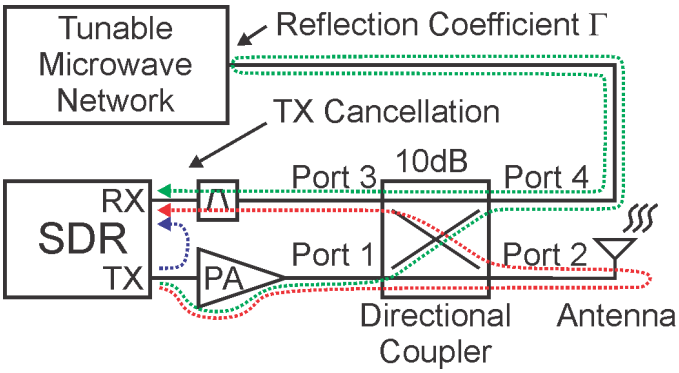

Fig. 1: Reflected Power Canceller Concept Used For Monostatic SDR-Based RFID Reader.

B. Prior Art in Transmit Cancellation in RFID Readers

Several major approaches to performing TX cancellation at RF in RFID readers have been previously proposed. One is vector modulation, in which a copy of the TX signal is extracted by a directional coupler, then phase shifted and amplitude adjusted such that it cancels any TX leakage in the RX path when coupled back into the latter. Reported approaches applied to UHF RFID include [3] [4] [5] [6]. The advantage here is that it is intuitively clear how the TX leakage is being cancelled. The disadvantage is typically that it requires a lot of relatively expensive components. For example, the active components described in [6] alone total about $70 using the lowest publicly available bulk pricing on Digi-Key.

Another approach is on-chip cancellation. One strategy is to drive the RX mixer LO port with a copy of the TX output signal in such a way that phase noise and TX leakage at baseband are considerably reduced [2]. After this, the remaining TX leakage can be high-pass filtered out in the baseband analog prior to the ADC. Another strategy was described in [7] in which a DC notch was established at

2573-7635 ©2018 IEEE. Digital Object Identifier 10.1109/RFID.2018.8376194.

the transimpedance amplifier following a passive-mixer-first receiver front end. The advantages with an on-chip approach are low board space requirements and low incremental cost. The chief disadvantage is the high fixed cost of the requisite custom ASIC development.

The final major approach discussed here is a reflected power canceller (RPC) approach, depicted in Fig. 1. In the RPC approach, a directional coupler is used to multiplex the TX and RX signals onto the antenna. At the fourth port of the directional coupler, a termination impedance with a suitable, often programmable, reflection coefficient Γ is presented such that the TX signal reflecting off of it is of precise magnitude and phase to cancel any TX leakage that finds its way to the input of the receiver. The RPC approach was originally proposed in the context of radar [8]. Later, this technique was applied to UHF RFID [9] and subsequently in [10] [11] [12]. The advantage with the RPC approach is that the circuitry involved can be composed of low-cost fundamental components such as variable capacitors, PIN diodes, or variable resistors. The disadvantages with this approach are that determining an efficient architecture for obtaining good coverage of possible suitable Γ is nontrivial and that it may consume a moderate amount of board area. In order to minimize both the fixed and variable costs of the transmit cancellation circuitry, this paper explores the RPC approach.

C. Prior Art in Tunable Microwave Networks

Each RPC is distinguished by the tunable microwave network (TMN) utilized at the fourth port of the directional coupler to generate the aforementioned Γ. In the 1970s and 1980s, TMNs were developed for use in automated RF load-pull testers. Many of these networks were characterized by the placement of PIN diodes in shunt configuration at various locations within a delay line network. Since a forward-biased PIN diode acts as a current-controlled resistor at microwave frequencies, the wave reflected from said PIN diode locally experiences a variable magnitude change but zero phase shift. The phase component of the network Γ is dictated by which PIN diode is actuated. Hence, phase and amplitude control of Γ were independent. Notable examples of such work were reported in [13] [14] and [15]. Such TMNs could be relatively large and power hungry.

Soon after the advent of UHF RFID, [9] reported an RPC-based UHF RFID "passive circulator" with a fixed TMN. Subsequently, a compact PIN diode based TMN approach was presented in [10] [12]; however, in each case, the method by which current was applied to the PIN diodes was not reported and tuning was applied manually. Furthermore, the resistive nature of forward-biased PIN diodes means that they can become a significant noise contributor to the system [10].

More recently, a RPC based TX leakage canceller using a network based on newly introduced digitally tunable capacitors (DTCs) was presented [11]. DTCs have the advantage of being low loss, and hence low noise. As capacitors, DTCs can in principle draw no static current, although in practice they draw on the order of 100uA each [16] [17]. Since their principal intended use is to tune antennas in mobile phones, DTCs in general tolerate watt-level power at their inputs with high linearity and are hence similarly suited for use in RFID systems. The main drawback of currently available DTCs is the limited resolution.

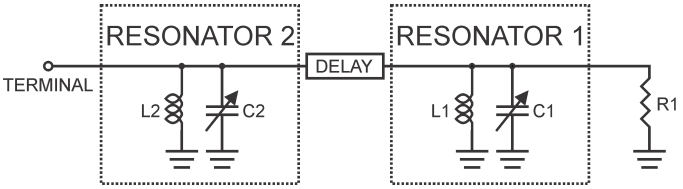

Fig. 2: Depiction of Basic Coupled Resonator Tunable Microwave Network.

This latter limitation became apparent in [11] in which a 2-DTC network was presented wherein each DTC had 5 bits of resolution. The resulting difference between worst-case received carrier power with no tuning and with tuning was 20dB. While this level of rejection was sufficient to improve the performance of the low phase-noise AS3992 reader ASIC used in [11], it is not in general sufficient for a custom low-cost software-defined RFID reader, as discussed below.

II. TMN Architecture and Principle of Operation

A. Motivation

The principal contribution of this paper is to describe a low-cost, easily tunable, high-resolution, DTC-based TX leakage cancellation scheme that is suitable for use in a low-cost software-defined radio (SDR)-based UHF RFID reader such as the one reported in [18]. Such a low-cost reader should work with a low-cost antenna, which would typically be specified with a maximum $|S11|$ of about -10dB. The exact phase and magnitude of the antenna reflection coefficient under any given condition is unknown save for the upper bound on its magnitude. Since the majority of the TX leakage will come from antenna reflections, the TMN Γ must be able to cancel leakage from all possible antenna reflection coefficients. The set of these coefficients can be viewed as a disk with radius of 0.3 at the center of a Smith chart. Due to the reciprocity of the directional coupler in Fig. 1, this translates into a requirement on the TMN Γ to cover the same disk of radius 0.3 with as many evenly spaced points as possible.

B. Basic Operation

The proposed TMN for the SDR RFID reader of [18] is a coupled resonator network of the type described in [19], which is depicted in Fig. 2. The design of such a network to achieve a desirable Γ coverage can be explained using the Smith admittance chart shown in Fig. 3. The points labeled "1" can be thought of as Γ realizable by Resonator 1. Choosing R1 to be less than 50Ω in Fig. 2 sets the middle point 1 of Fig. 3 to an advantageous location left of the dashed blue circle. Shunt inductance L1 then sets the location of the topmost point 1. Increasing via actuation the shunt capacitance C1 then traces a set of points labeled "1" from top to bottom along the Smith

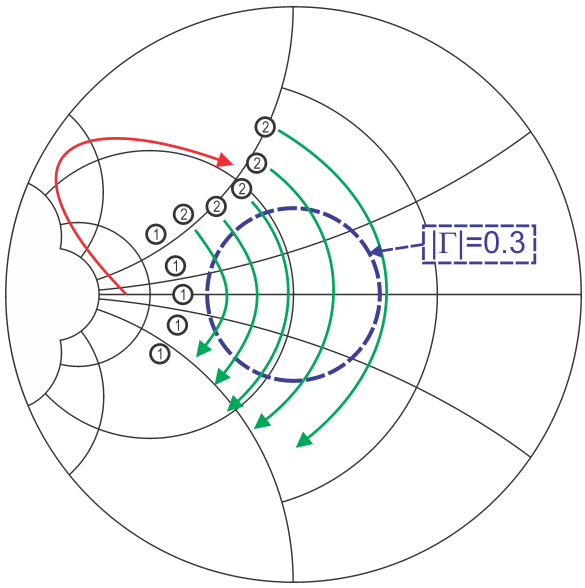

Fig. 3: Depiction of Basic Coupled Tunable Microwave Network Reflection Coefficient Coverage.

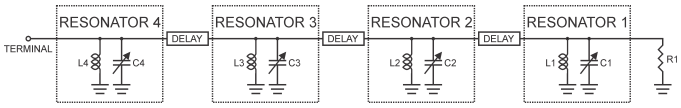

Fig. 4: Depiction of Four-Coupled Resonator Tunable Microwave Network.

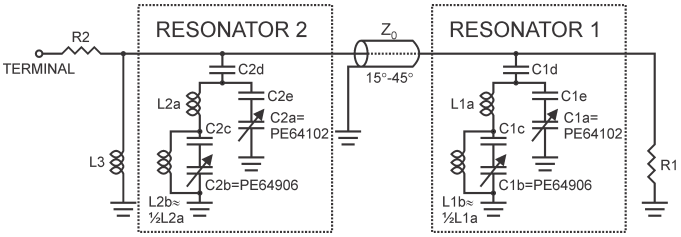

Fig. 5: Proposed Tunable Microwave Network Circuit.

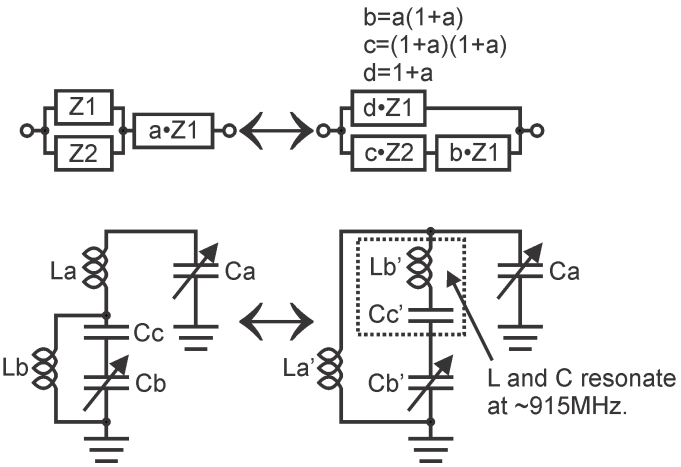

Fig. 6: Impedance Transformations in Tunable Microwave Network Circuit.

chart admittance curve. In order to prepare to completely cover the disk of $|\Gamma| < 0.3$ with realizable reflection coefficients, the delay line rotates the set of points 1 by about 45° to the set of points labeled "2", with said rotation depicted by the red curve. Finally, increasing the value of the shunt capacitance of Resonator 2 sweeps a set of reflection coefficients across the disk of $|\Gamma| < 0.3$ over the set of admittance curves crossed by points "2", as depicted by the green curves. While a transmission line was used to realize the interstage delay in this project, an inductor may also be used, as depicted in [19].

C. Increasing Resolution

It is derived in [18] that the cancellation ratio of the TMN should be at least 50dB in order to keep the residual phase noise of the SDR ASIC used in [18] well below the desired reader sensitivity level. The 5-bit resolution of currently available DTC devices employed in the simple two-resonator network of [19] would yield $(2^5)^2 = 1024$ points, sufficient for 30dB cancellation if the realizable Γ could be made to exactly and uniformly cover a circle. Since neither metric can be perfectly achieved, a cancellation ratio of 20dB as reported in [11] is more realistic.

1) More Coupled Resonators: One way to possibly solve this problem is to add more coupled resonators in series, as shown in Fig. 4. A similar architecture is reported in [20] and implemented on a custom CMOS SOI ASIC targeting a general full-duplex radio application. One reason why such an architecture is disadvantageous is that the increased number of state variables will complicate, and likely slow, any convergence algorithm utilized relative to a two-capacitor solution.

Another disadvantage in the context of resolution-limited DTC components is that subsequent curve sweeps across the Smith chart due to potential shunt capacitances C3 and C4 are of the same resolution as original shunt capacitances C1 and C2, assuming that the highest resolution available DTCs are used in each case. If the C3 and C4 curves end up being collinear with those of C1 and C2, the resolution of the resulting network can only increase by one bit. If the C3 and C4 curves do not end up being collinear with those of C1 and C2, the resolution of the resulting network can increase by more than one bit, but the resulting set of realizable Γ is observed to be effectively randomly distributed. The upshot of this situation is that the maximum spacing between realizable Γ is considerably larger than if the Γ were to be roughly uniformly distributed.

2) Subranging: The solution architecture developed to increase the resolution of the DTC-based coupled resonator TMN while keeping the number of effective capacitors the same is shown in Fig. 5. In order to increase the number of effective bits, the inductors in the LC tanks were split and used to provide an upwards impedance transformation of another set of DTCs. Judicious choice of the upwards

impedance transformation permits C1b and C2b to act as subranging capacitors to C1a and C2a, respectively. The relevant transformations are covered in [21] and are depicted in Fig. 6. Such a transformation is called a "tapped inductor resonator" [22] or a "tapped inductive impedance transformer" [23]. Considerations of the transforms in Fig. 6 are important because they reveal a parasitic inductance Lb' that must be tuned out by an extra fixed capacitance Cc' near the frequency of operation. The proposed network also contains extra fixed capacitances C1d and C2d which compress the space of realizable Γ to make them more strictly and uniformly cover the disk with radius of 0.3 on the Smith chart, and C1e and C2e, which help tune out parasitic inductances. In this case, $(2^5)^4 = 1048576$ Γ may be realized, corresponding roughly to a maximum achievable cancellation ratio of 60dB. However, since the set of realized Γ will not perfectly cover the Smith chart disk of $|\Gamma| < 0.3$, one can expect the worst-case cancellation ratio to be more along the lines of 50dB, which is still 30dB greater than in [11].

C1a and C2a were implemented by Peregrine PE64102 DTCs, while C1b and C2b were implemented by PE64906 DTCs. The total cost of the DTC components based on the lowest publicly available bulk price on Digi-Key is $2.30. The Johanson directional coupler utilized is $0.46 and the the RF-grade inductors utilized cost $0.67 when quoted in the same manner. However, the use of RF-grade passives was done to guarantee first-pass success of the design and lower-quality inductors can clearly be used due to the inherent lossiness of the TMN. Other passive component costs are negligible. The total cost of the TMN components in bulk is therefore expected to be less than $4 while total leakage current should be less than 1mA, according to the DTC data sheets.

D. Simulated Results

The simulated coverage of the proposed TMN with extracted PCB parasitics is shown in Fig. 7. As is evident, the space of realizable TMN reflection coefficients covers the disk of $|\Gamma| < 0.3$ and more. A computational analysis of this set of points reveals that the largest distance of any reflection coefficient to a TMN-realizable reflection coefficient within the disk of $|\Gamma| < 0.3$ is very close to 0.001, indicating a worst-case cancellation ratio of 50dB (which does not count the 10dB improvement already afforded by specifying the maximum antenna |S11| as -10dB). Note that these simulation results are from a pre-implementation network - the capacitor values were changed post-implementation to account for discrepancies between the extracted PCB model and the actual hardware.

III. Tuning Algorithm

A. Operation

For the purposes of the tuning algorithm, the main and subranging capacitors of each resonator are operated together as a 10-bit DTC. Therefore, below, only composite tuning capacitors C1 and C2 are discussed, but in reality all 4 DTC ASIC are being actuated.

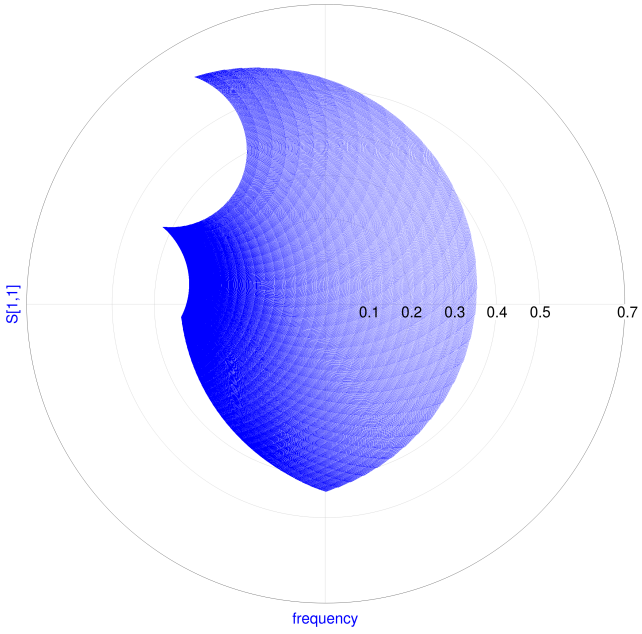

Fig. 7: Simulation of Tunable Microwave Network Reflection Coefficient Coverage.

1) Considered Non-Blind Algorithm: At the commencement of this project, it was desired to implement a gradient descent algorithm that utilized knowledge of the Jacobian matrix relating the TMN C1 and C2 settings to the real and imaginary parts of the realized Γ. The idea was that the more information about the system that was utilized in the computation, the faster the algorithm would converge. This concept worked well in simulation and could be compactly implemented in the FPGA of [18].

However, the static phase relationship between the SX1257 SDR radio TX and RX LOs in [18] turns out to randomly vary from chip power-up to chip power-up, seemingly uniformly distributed across the entire 360° phase range. The reason for this is ultimately that the TX and RX frequency synthesizers in the SX1257 radio chip used in [18] are independent fractional-N PLLs. Therefore, the aforementioned {C1,C2} to Γ mapping as observed by the reader digital baseband in fact rotates randomly. As such, at least some blindness on the algorithm for tuning this implementation is required. For a different SDR ASIC, however, a faster nonblind approach could potentially be utilized.

2) Employed Algorithm: The algorithm driving the RPC TMN is depicted in Fig. 8. It is a fully blind algorithm that uses independent changes in C1 and C2 to effectively compute the local gradient of the TX leakage at the SDR ASIC RX input and to actuate C1 and C2 in such a way as to minimize this leakage. This algorithm is implemented on the FPGA in [18] and consumes 222 Logic Elements and 16 9-bit multipliers. It is important to note that due to its implementation at digital baseband, the algorithm only has the digital DC signal as

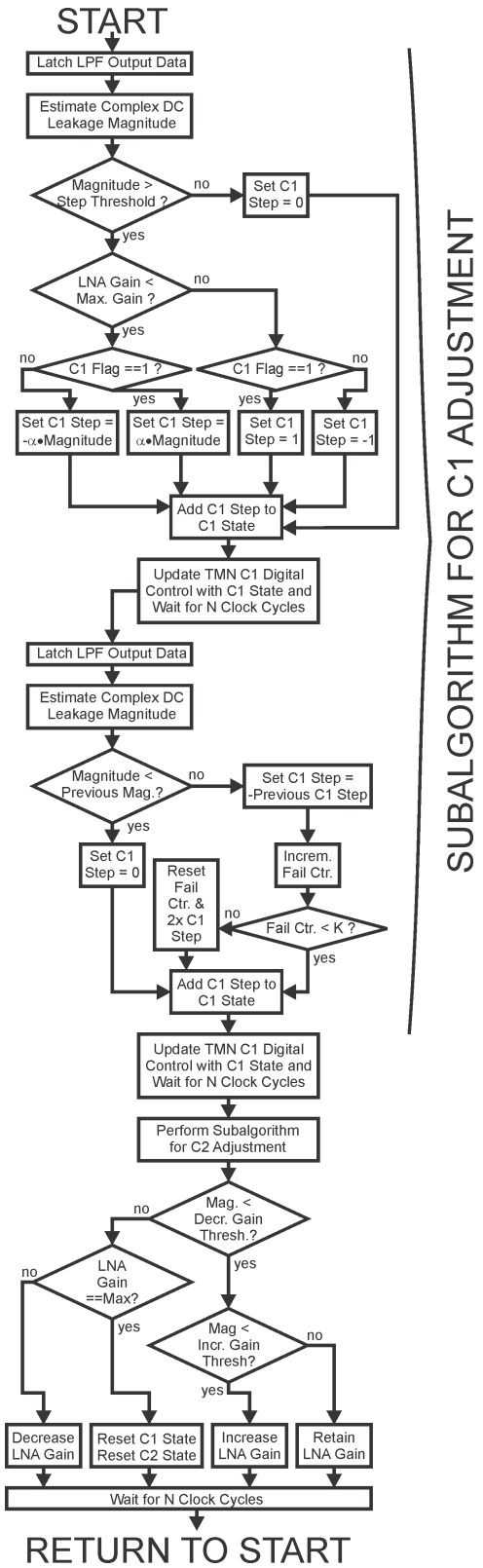

Fig. 8: Depiction of Tunable Microwave Network Tuning Algorithm.

a proxy for the TX leakage at the SDR ASIC RX input. Furthermore, because the uncancelled TX leakage will easily saturate the SDR ASIC RX at the gains required to demodulate a tag backscatter signal at range, the tuning algorithm must progressively step up the SDR ASIC RX gain as TX leakage at the input is reduced. It was ultimately found that 3 gain settings were required to achieve good performance.

The algorithm estimates the magnitude of the TX leakage at the receiver input using the approximation: $\max(\text{DC\_I},\text{DC\_Q})+\frac{1}{4}\min(\text{DC\_I},\text{DC\_Q})$ [24] right bit shifted by a number of bits commensurate with the RX gain. Here, DC_I and DC_Q are the I and Q components of the down-converted TX leakage, respectively. If this magnitude estimate is greater than about -50dBm at the SDR ASIC input, the algorithm executes. If not, the algorithm and all SPI communications to the DTC and SDR ASIC are shut down to avoid algorithmic chatter and glitching on the DTC ASICs, coupling from which is observed to easily overwhelm the received tag backscatter signal at range. If the LNA gain is less than its maximum, the steps taken by the algorithm are proportional to the estimated magnitude. Otherwise, C1 and C2 are only incremented and decremented by 1 to ensure that any exploratory steps taken do not result in TX leakage saturating the receiver. The -50dBm comes about because expected uncancelled TX leakage at the SDR ASIC input for an antenna $|S11|$ of -10dB is about 0dBm. and -50dBm is this level minus the requisite cancellation ratio.

C1 and C2 flags are utilized to store the signs of the roughly orthogonal components of the local gradient of the TX leakage. Functionally, these flags control whether C1 and C2 are incremented or decremented on each step. If the algorithm sees that the baseband DC magnitude is decreasing on each iteration, the flags are kept constant. If the baseband DC magnitude increases on any step, the previous step is reversed and the relevant C1 and C2 flag is flipped so that the corresponding capacitor is actuated in the opposite direction on the next algorithmic interval. Also if the baseband DC magnitude increases on any step, a "fail counter" increments. When the "fail counter" reaches a high enough value, indicating that the algorithm may be trapped in a local minimum, the next C1 or C2 step value is temporarily doubled in an attempt to escape. The "fail counter" is reset to zero at any one of these doublings, or when DC TX leakage magnitude decreases.

After actuating C1 and C2 (and possibly reversing this actuation if TX leakage magnitude increased as a result), the TX magnitude estimate is compared against a set of thresholds which dictate whether the LNA gain will be changed on the next iteration. If the TX magnitude is too high and the RX gain is at minimum, the DTC capacitors are reset in order to bound the TX leakage level to avoid ever saturating or damaging the SDR ASIC RX chain.

B. Simulated Results

The proposed algorithm was simulated in Octave along with the pre-implementation reflection coefficient set shown in Fig. 7. Ninety-six uniformly spaced antenna reflection coefficients were selected from over the centered Smith chart disk with radius of 0.3 and used to generate a TX CW input to the

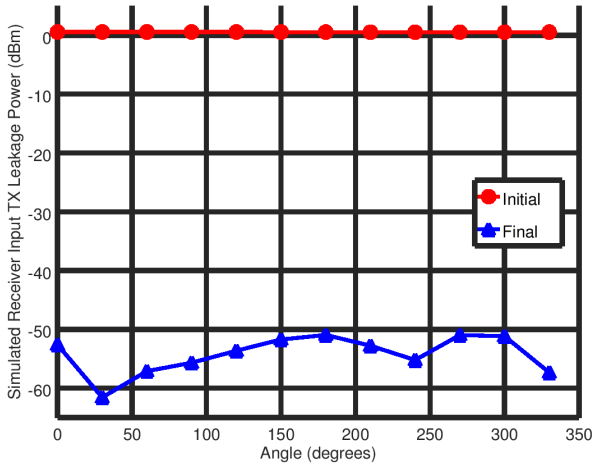

Fig. 9: Simulated TX Leakage at SDR ASIC Input Before and After (30ms) Algorithm Execution.

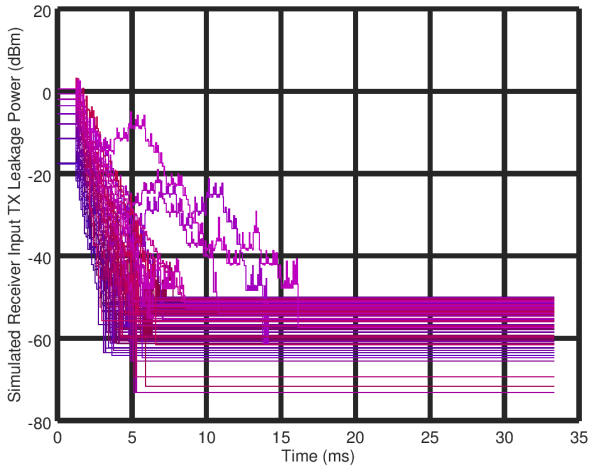

Fig. 10: Ensemble Plot of Simulated Algorithm Convergence Behavior. (Each line is an individual simulation run.)

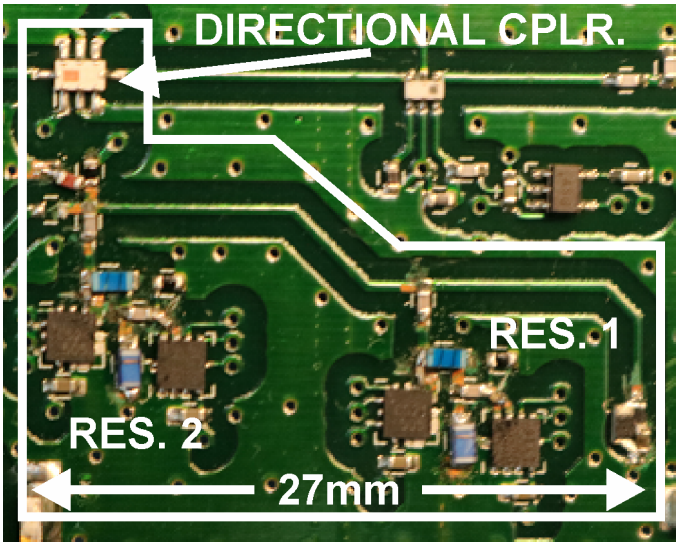

Fig. 11: Picture of TMN on SDR RFID Reader board.

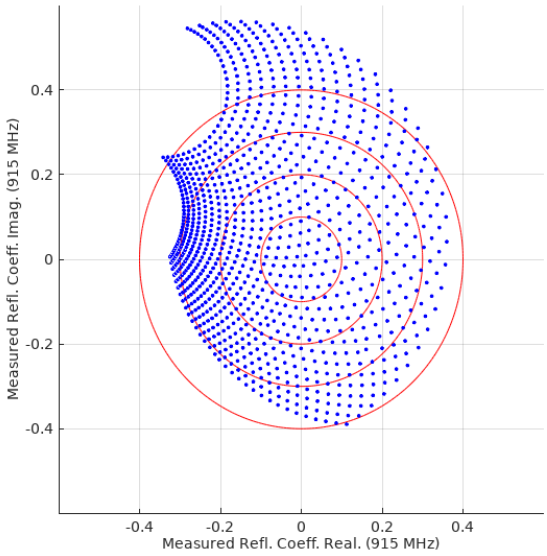

Fig. 12: Measured TMN Coverage at 915MHz for Coarse Capacitor Tuning.

receiver. Fig. 9 shows the before-and-after SDR ASIC input-referred TX leakage for those antenna reflection coefficients with magnitude of 0.3, while Fig. 10 is a plot showing the convergence behavior for each antenna reflection coefficient. It can be seen in Fig. 9 that TX leakage referred to the input of the SDR ASIC is reduced by over 50dB to below -50dBm in each instance. The median time to reduce SDR ASIC input-referred TX leakage to below -50dBm is 4.18ms, while the maximum time is 16.16ms. It is important to note that the algorithm continues to track residual TX leakage at DC baseband after the initial convergence. Also, the algorithm state is held between RFID operations, so only minimal convergence adjustments are needed during these intervals.

Quantities here and in Section IV are referred to the SDR ASIC RX input for several reasons. First, this the termination point for most dominant TX leakage paths on the PCB, as shown in Fig. 1. Assuming a perfect ASIC, the TX leakage must be cancelled here. Second, it is important to keep track of the TX leakage power at this point to ensure that the SDR ASIC is neither being saturated nor damaged. If required, all SDR ASIC-RX-input-referred quantities can be referred to the overall reader input by adding about 19dB to account for the 10dB directional coupler loss, 6dB input attenuator, and 3dB BPF on the reader in [18].

IV. Implementation and Measurements

The TMN was implemented and tested *in situ* on the associated SDR RFID reader in [18]. A close-up of the TMN circuit is shown in Fig. 11. The portion of the TMN circuit comprised of the DTCs and other passives (minus the directional coupler) fit into a square measuring 27mm by 25mm. The measured

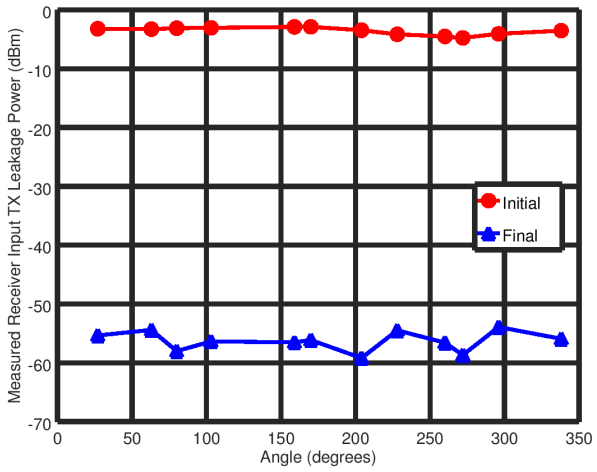

Fig. 13: Measured Initial and Final TX Leakage referred to SDR ASIC Input.

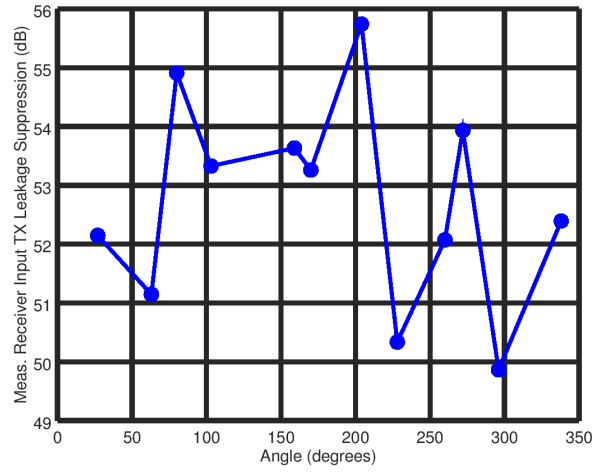

Fig. 14: Measured TX Leakage Cancellation Ratio (Suppression).

Smith chart coverage of the TMN at 915MHz for tuning of the two coarse DTCs is shown in Fig. 12. The coverage is similar from 902MHz-928MHz, with only a few tiny slivers of the disk of $|\Gamma|$ <0.3 uncovered at 902MHz, which could easily be fixed by a subsequent retuning if absolutely necessary. All other measurements described herein are performed at 915MHz with no loss of generality.

The TX leakage cancellation performance was evaluated in a manner similar to that described in [5] and [6]. A series of 1" x 1" dummy boards was loaded with static passive networks to generate 12 reflection coefficients around the Smith chart circle at a magnitude of ≈0.3 and each dummy board was attached to the antenna port of the RFID reader in [18] in turn. Due to the ad hoc nature of the dummy board tuning, the realized angles are somewhat randomly distributed from 0° to 360°. In each instance, the TX was set to output a CW tone and the tuning algorithm was allowed to run 4 times from its initial

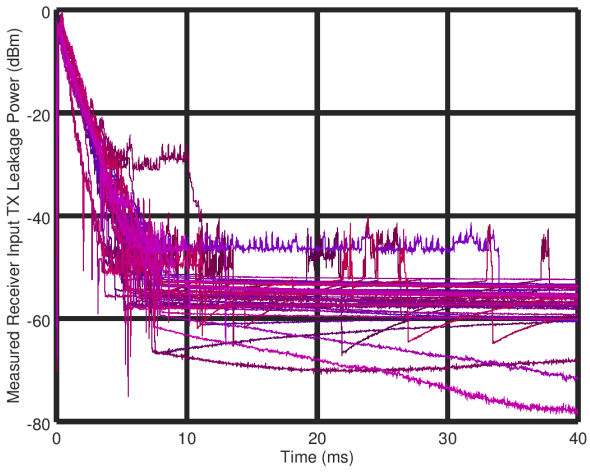

Fig. 15: Measured Ensemble Convergence Behavior. (Each line is an individual measurement run.)

state. During this time, data was collected from the digital outputs and gain control input of the SDR ASIC with a logic analyzer. The captured digital data was then postprocessed and input-referred in Octave using models of the FPGA DSP filters in [18] and the receiver gain.

The mean pre- and post-cancelled TX leakage power at the SDR ASIC RX input as a function of antenna port reflection coefficient angle is shown in Fig. 13. For clarity, the cancellation ratio, i.e. the difference between the two curves in Fig. 13, as a function of angle is presented in Fig. 14. Greater than 49.8dB suppression was achieved at each angle. Note that, as discussed in [18], it was required to reduce TX output power to 26dBm from a proposed 29dBm to avoid problematic distortion arising from the reader antenna diversity switch. As such, the initial power shown in Fig. 13 is around -3.5dBm (26dBm output power-10.5dB reflected from dummy board-19dB from reader RX input network=-3.5dBm).

The ensemble convergence behavior of all of the measured runs is shown in Fig. 15. One can see in Fig. 15 several runs with increased bursts of TX leakage power after the initial convergence. These runs are all from angle=27°, indicating an atypical scenario. For this dummy board, input-referred error drifted higher after an initial convergence, requiring a periodic correction by the algorithm. Methods to circumvent problems arising from such behavior can be trivially implemented, if required. For example, since the error rises over the course of 10ms or so, one could simply disable algorithmic convergence during backscatter reception of a packet. Disregarding these scenarios, the maximum measured time to convergence is 34ms. The median time to achieve -50dBm SDR ASIC-input-referred error is 7.29ms. It should be noted that these convergence times are on par with those reported by [6] for a similar cancellation ratio and residual power limit but at a much lower BOM cost and board area for the cancellation network.

As discussed in Section I-A, ultimately the TX leakage

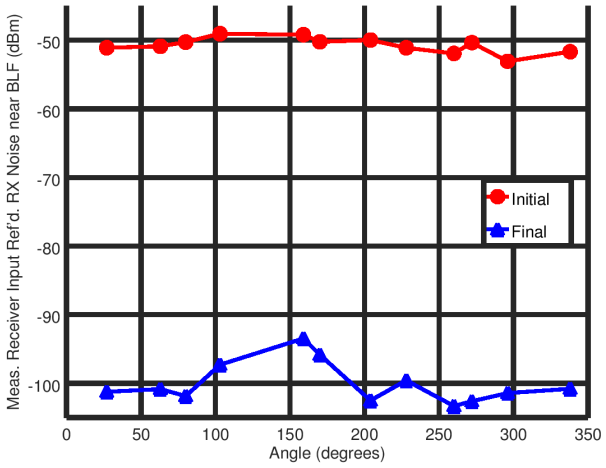

Fig. 16: Measured Initial and Final RX Noise near BLF referred to SDR ASIC Input.

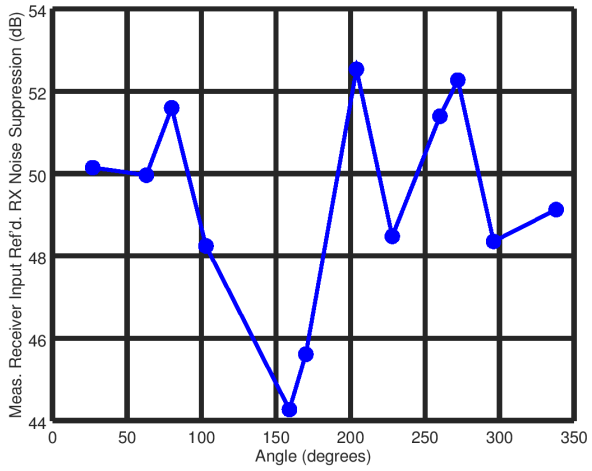

Fig. 17: Measured RX Noise Suppression.

cancellation method must reduce the phase noise seen by the RX path or else the backscatter signal cannot be received at range. As shown in Figs. 16 and 17, the noise seen at the output of the RX channel filter of [18], referred to the SDR ASIC input, is suppressed by over 44dB. In most cases, the -98.5dBm SDR ASIC input-referred phase noise target of [18] was achieved. As in the other measurements, 4 runs were averaged to obtain these plots.

V. Conclusion

A low cost adaptive reflected power canceller with a sub-ranging DTC-based tunable microwave network (TMN) is presented. The proposed system achieves a convergence time similar to recently reported works despite being much lower in cost and size. Ultimately, this design enabled a fully-functional, low-cost SDR UHF RFID reader prototype. Future work entails estimating the TX/RX LO phase relationship of the associated SDR ASIC so that this information, combined with knowledge of the realizable reflection coefficients of the TMN, can be used to drive a nonblind tuning algorithm that achieves even faster convergence than that presented herein.

References

[1] "EPC radio-frequency identity protocols generation-2 UHF RFID specification for air interface protocol for communications at 860MHz - 960MHz version 2.0.1 ratified," 2015.

[2] S. Chiu *et al.*, "A 900 MHz UHF RFID Reader Transceiver IC," *IEEE J. Solid-State Circuits*, vol. 42, pp. 2822–2833, Dec. 2007.

[3] J.-W. Jung *et al.*, "TX Leakage Cancellation via a Micro Controller and High TX-to-RX Isolations Covering a UHF RFID Frequency Band of 908-914MHz," *IEEE Microwave and Wireless Comp. Letters*, vol. 18, pp. 710–712, Oct. 2008.

[4] D. P. Villame *et al.*, "Carrier Suppression Locked Loop Mechanism for UHF RFID Readers," in *Proc. IEEE Int. Conf. RFID*, Apr. 2010, pp. 141–145.

[5] I. Mayordomo *et al.*, "Implementation of an Adaptive Leakage Cancellation Control for Passive UHF RFID Readers," in *Proc. IEEE Int. Conf. RFID*, Apr. 2011, pp. 121–127.

[6] K. Kapucu *et al.*, "A Fast Active Leakage Cancellation Method for UHF RFID Readers," in *Proc. IEEE Int. Conf. RFID*, May 2017, pp. 182–186.

[7] Q. Guo *et al.*, "A Novel Adaptive Leakage Suppression Method for UHF RFID Reader," in *Proc. IEEE Int. Conf. RFID*, May 2017, pp. 187–192.

[8] P. Beasley, A. Stove, B. J. Reits, and B. As, "Solving the Problems of a Single Antenna Frequency Modulated CW Radar," in *Proc. IEEE Radar Conf.*, 1990, pp. 391–395.

[9] W.-K. Kim *et al.*, "A Passive Circulator for RFID Application with High Isolation using a Directional Coupler," in *Proc. 2006 European Microwave Conference*, Sep. 2006, pp. 196–199.

[10] T. Brauner and X. Zhao, "A Novel Carrier Suppression Method for RFID," *IEEE Mic. and Wireless Comp. Letters*, vol. 19, pp. 128–130, Mar. 2009.

[11] M. Koller and R. Kung, "Adaptive Carrier Suppression for UHF RFID using Digitally Tunable Capacitors," in *2013 European Microwave Conference*, Oct. 2013, pp. 943–946.

[12] A. J. S. Boaventura *et al.*, "The Design of a High-Performance Multisine RFID Reader," *IEEE Trans. Microwave Theory and Tech*, vol. 65, pp. 3389–3400, Sep. 2017.

[13] B. W. Leake, "A Programmable Load for Power and Noise Characterization," in *Microwave Symposium Digest, 1982 IEEE MTT-S International*, June 1982, pp. 348–350.

[14] B. M. Albinsson *et al.*, "A New Programmable Load for Noise Parameter Determination," *IEEE Trans. Microwave Theory and Tech.*, vol. 39, pp. 216–223, Feb. 1991.

[15] L. Klapproth *et al.*, "A Programmable Load for Noise Characterization," in *ARFTG Conference Digest-Spring, 49th*, June 1997, pp. 155–160.

[16] *Product Specification: PE64102*, Peregrine Semiconductor, 2013.

[17] *Product Specification: PE64906*, Peregrine Semiconductor, 2017.

[18] E. A. Keehr, "A Low-Cost Software-Defined UHF RFID Reader with Active Transmit Leakage Cancellation," in *Proc. IEEE Int. Conf. RFID*, Apr. 2018.

[19] R. Whatley *et al.*, "CMOS Based Tunable Matching Networks for Cellular Handset Application," in *Proc. IEEE Intl. Micr. Symp.*, Jun. 2011, pp. 1–4.

[20] B. Debaillie *et al.*, "RF Self-Interference Reduction Techniques for Compact Full-Duplex Radios," in *IEEE 81st Veh. Tech. Conf. Spring*, May 2015, pp. 1–6.

[21] O. J. Zobel, "Theory and Design of Uniform and Composite Electric Wave-filters," *Bell Sys. Tech. J.*, vol. 2, pp. 1–46, Jan. 1923.

[22] T. H. Lee, *The Design of CMOS Radio-Frequency Integrated Circuits*, 2nd ed. Cambridge, UK: Cambridge University Press, 2004.

[23] T. A. Gadwa, "An Impedance Matching Transformer," *QST*, vol. 27, pp. 22–39, Feb. 1943.

[24] "DSP Trick: Magnitude Estimator," https://www.dspguru.com/dsp/tricks/magnitude-estimator, accessed: 2017-11-25.